

Topological Glasses

Michieletto Davide, Prof. Turner Matthew

University of Warwick, Complexity Centre, Zeeman Building

(Dated: September 10, 2012)

Abstract. In this paper we perform 3-dimensional molecular dynamics simulations of ring polymers in solution and in the presence of a fixed network of obstacles. Both static and dynamic properties of such solutions are studied throughout in order to give some insights on the relationship between topological properties and macroscopic behaviour. The longest rings were composed of $M = 1024$ monomers per chain and observed at coil packing fraction $\phi = 1.25$. The size of isolated rings has also been found to scale as $M^{1/2}$ when embedded in a network of fixed obstacles (mesh), according with previous theoretical considerations. Moreover, the presence of the mesh leads naturally to the study of local intra-ring and inter-ring entanglements. Here, we propose a new method to identify, unambiguously, the existence of inter-ring penetrations and to relate it to the dynamics of such rings.

I. INTRODUCTION

The study of polymers in solutions has always been one of the most challenging problems in soft matter physics. Polymers are substances consisting of long molecular chains which are formed by repeating simple units connected by bonds. An helpful image to keep in mind is some sort of long, coiled, three-dimensional thread, or pearl necklace. Artificially made polymers can have up to millions of units ($M \sim 10^4 - 10^6$) while natural polymers can be even longer, for instance DNA molecules can have up to 10^{10} nucleotides. Such long molecules appear in different forms: linear, branched or closed. In this paper we are interested on the last type, closed polymers, or rings. Because of their shape (imagine to take a long pearl necklace and join the two ends) they can have very peculiar properties and configurations, as being threaded through each other (see fig. 1), which cannot be described by theories based on linear polymers.

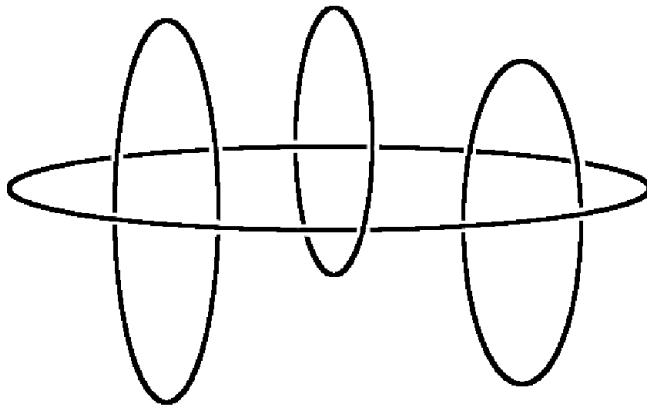


FIG. 1: Cartoon of a possible configuration of ring polymers. The horizontal ring is threaded by the two external ring and passes through the middle one. Such configuration clearly causes a strong constraint on its free diffusion which cannot be explained using standard theories based on linear polymers.

During the last decade the development of tools for synthesizing polymers has been making easier the experimental preparation of solutions made of pure ring polymers [11]. At the same time, the increasing availability of computational power has been facilitating the simulations of large

number of long molecules. Recent experimental and computational observations shed light on how polymeric structure and dynamics are related to each other[1, 4, 8, 9, 15], often supporting theoretical conjectures provided more than two decades ago by Doi, Edwards, De Gennes and Cates[2, 5, 7]. Entanglement effects have been largely studied for linear polymers. Nevertheless, as we have already suggested, the same results cannot be extended to the case of closed, unknotted and unlinked polymers which can show both entanglement and threading. In this paper we will use the word ‘entanglement’ to indicate a generic topological interaction which occurs when pieces of polymers constrain the motion of each other, while we will use ‘threading’ or ‘penetration’ to refer to a precise type of entanglement as sketched in fig. 1. Intra-chain and inter-chain entanglements in both linear and closed polymer solutions has always drawn attention from both theoretical and experimental communities. How these topological constraints affect physical properties of the solutions as the viscosity? It has been suggested that, in the case of dense solutions of ring polymers, the threading of a chain through another, can result in dramatic slowing of the polymer dynamics while open chains cannot interact in the same way, due to their different topology. In the limit of long closed loops, as in the case of bacterial DNA or artificial long polymers, one might expect highly inter-penetrated state to arise. The solution of rings would have properties very different from those of the liquid state, and closer to those of a solid state. Unfortunately, such states have not yet been unambiguously identified.

We are therefore interested on systems in which very long, closed polymers are prepared in semi-dilute solution in which the rings are swollen by the solvent and interact topologically with other chains. Here, we decide to carry out our simulations embedding the whole system of rings in a three dimensional grid of obstacles, reminiscent of a very ordered mesh, or gel. The presence of the mesh has various advantages. It mimics experimental systems used in DNA electrophoresis, or polymeric blends where one species is linear but much longer and heavier than the other type. More than that, if we take the ‘lattice size’ of the gel to be smaller than the average linear extent of the polymers, it is very unlikely that they collapse inside a unit cell and segregate from one-another, as already observed in simulations of ring melts[17]. In this way, we enhance the topological interactions among the chains and aim to study a new state of matter, called a ‘topological glass’. This state is indistinguishable from the liquid state locally, but the motion on macroscopic scales would be dramatically slowed, due to topological constraints.

The present paper is organised as follows: in section II we describe the model and how it is implemented numerically; in section III we give a brief introduction about the theoretical concepts and the observables useful throughout the paper. In section IV we focus on dilute systems and on the differences between dynamic and static properties of the rings in presence or absence of the gel. In section V we study system in overlapping regime (higher coil density) and in section VI, we take advantage of the presence of the lattice of obstacles to suggest new way of measuring inter-chains penetrations and unambiguously identify threading from generic entanglement. In section VII we then present our conclusions.

II. THE MODEL AND THE SIMULATION ENGINE

The dynamic and static properties of the polymers are studied using fixed-volume and constant-temperature molecular dynamics (MD) simulations via LAMMPS engine. Following the pioneering work of Kremer and Grest [10] we use a bead-spring model to take into account chain connectivity, excluded volume interactions, chain stiffness and to preserve the topology of the polymer chains.

In particular, the intra chain potential is given by the following Hamiltonian:

$$H_{intra} = \sum_{i=1}^M \left[U_{FENE}(i, i+1) + U_b(i, i+1, i+2) + \sum_{j=i+1}^M U_{LJ}(i, j) \right] \quad (1)$$

where M is the number of beads in each ring. Each monomer has nominal size σ and position \mathbf{r}_i , while the distance between two monomers i and j is given by $d_{i,j} = |\mathbf{r}_i - \mathbf{r}_j|$. The first term in eq. (1) is the ‘Finitely Extensible Non-linear Elastic’ model for the bonds:

$$U_{FENE}(i, i+1) = \begin{cases} -\frac{k}{2} R_0^2 \ln \left[1 - \left(\frac{d_{i,i+1}}{R_0} \right)^2 \right] & , d_{i,i+1} < R_0 \\ \infty & , d_{i,i+1} > R_0 \end{cases} \quad (2)$$

where $R_0 = 1.5 \sigma$, $k = 30 \epsilon / \sigma^2$ and the thermal energy $k_B T$ is set to ϵ . The FENE potential is a non-linear generalisation of the harmonic potential and it is now largely used in molecular simulations since it forbids the beads to be more than R_0 further apart, and therefore forbids inter-chains crossings (not accounted by a simple harmonic spring). The bending energy, or stiffness term, takes the standard Kratky-Porod form (discretized worm-like chain) [16]:

$$U_b(i, i+1, i+2) = \frac{k_B T \xi_p}{\sigma} \left[1 - \frac{\mathbf{d}_{i,i+1} \cdot \mathbf{d}_{i+1,i+2}}{d_{i,i+1} d_{i+1,i+2}} \right] \quad (3)$$

where ξ_p is the persistence length of the chain which is fixed at 5σ . Polymers are significantly bent by thermal fluctuations at contour lengths larger than the Kuhn length $l_k = 2\xi_p$. Here, the persistence length ξ_p is always assumed to be much smaller than the total length of the chain, so that the chains resemble a flexible polymer, rather than a rigid rod. The Lennard-Jones potential has the ‘cut and shifted’ form, which correspond to purely repulsive interactions:

$$U_{LJ}(i, j) = \begin{cases} 4\epsilon \left[\left(\frac{\sigma}{d_{i,j}} \right)^{12} - \left(\frac{\sigma}{d_{i,j}} \right)^6 + 1/4 \right] & , d_{i,j} < \sigma 2^{1/6} \\ 0 & , d_{i,j} > \sigma 2^{1/6}. \end{cases} \quad (4)$$

This regulates also all the pair interactions between monomers belonging to different chains or with the fixed mesh. According to the inter-chain Hamiltonian:

$$H_{inter} = \sum_{I=1}^{N-1} \sum_{J=I+1}^N U_{LJ}(i, j) \quad (5)$$

and the chain-mesh Hamiltonian:

$$H_{mesh} = \sum_{I=1}^N U_{LJ}(k, i) \quad (6)$$

where N is the number of chains in solution. The indexes i and j run over the beads in the chains, respectively, I and J , and k runs over the number of beads forming the mesh.

A. Simulation Details

Here we consider solutions with different packing fraction $\phi = \langle v \rangle N/V$, where $\langle v \rangle$ is the average volume of the chains, N the number of chains and V the volume of the system, spanning from non overlapping regime $\phi < 1$ to overlapping one $\phi > 1$. The polymers have contour length $L_c = M\sigma$. The box in which the solution evolves has periodic boundary conditions and linear size L . The gel is modelled via a collection of partially overlapping beads forming a cubic lattice with lattice constant $l_s = 10 \sigma$. The system dynamics is integrated using LAMMPS engine in the canonical ensemble (NVE), i.e. constant number of particles, volume and energy, and with a Langevin thermostat at target temperature $\bar{T} = 1 \epsilon$. The elementary discrete step time is chosen to be $\Delta t = 0.01 \tau_{LJ}$ where $\tau_{LJ} = \sigma(m/\epsilon)^{1/2}$ is the Lennard-Jones time, m is the mass of the beads (set to 1) and the friction coefficient correspond to $\gamma/m = 1 \tau_{LJ}^{-1}$. It is important to notice that the solvent is not explicitly introduced in the system but it is taken into account via the over-damped dynamics implicit in the Langevin thermostat and related friction term. Using the fluctuation-dissipation theorem one is then able to control the strength of the thermal noise driving the motion of the beads.

B. Preparation of the Samples

The simulation samples are usually prepared in a far-from-equilibrium configurations simply in order to fit a big number of monomers in a relatively small box. The strategy we have chosen consists of folding each ring across itself a sufficient number of times so that the linear extension of the ring is smaller than the linear size of the whole box. After this we thread each folded ring through the gaps left by the cubic lattice, as shown in fig. 2.

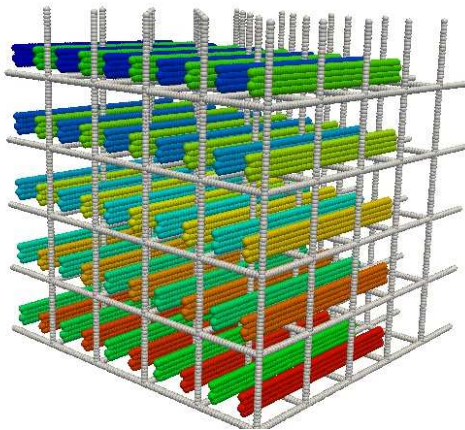


FIG. 2: Preparation of the sample with $N = 50$ rings with $M = 256$ beads each. Each polymer is folded on itself four times, while remaining a closed ring, before being threaded into the gel.

Since this is a very unnatural configuration, the systems are always allowed to evolve until the center of mass of the chains have travelled several times the average size of the polymers, or in other words, we wait several relaxation times defined as $\tau = \langle R_g^2 \rangle / D_{CM}$. For dense preparations this requires an equilibration time of the order of $10^6 \tau_{LJ}$. More precisely, we choose to switch off the Lennard-Jones repulsion between monomers belonging to the same ring and evolve the first few

thousand time-steps using a soft repulsion potential $U_{soft}(i, j) \sim A(1 + \cos \pi d_{ij}/2^{1/6}\sigma)$ for $d_{ij} \leq \sigma$, in order to avoid computational singularities. This method has been already used in [10] in the case of linear polymers. When applied to rings it gives a non-null probability (depending on A) that the chain crosses itself, generating a non-trivial knot. In order to avoid these unwanted configurations we check the presence of non-trivial links before we switch back on the Lennard-Jones repulsion used to equilibrate the system. It is worth to mention that once the L-J potential is active between every pair of monomers, the combination of L-J and FENE potential forbids any inter and intra chains crossings and therefore it conserves the topological state during the whole simulation. In fig. 3 we show two examples of configurations after the equilibration.

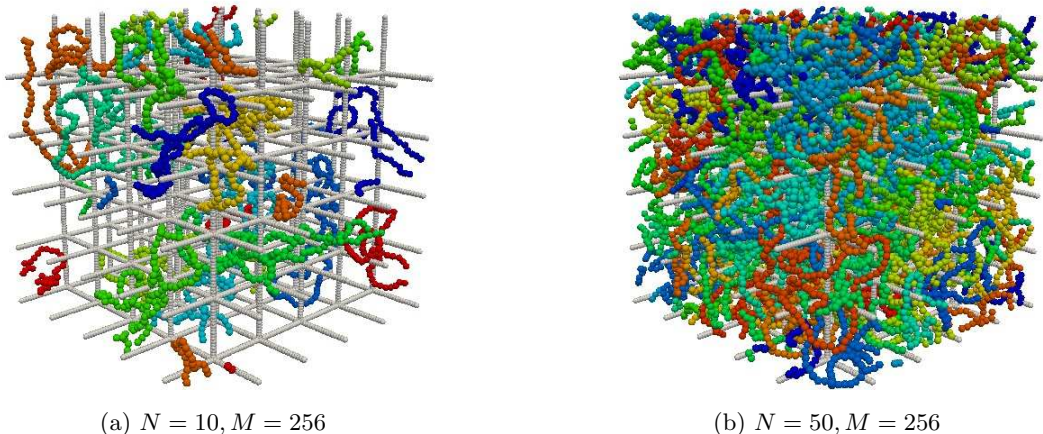


FIG. 3: Examples of equilibration configurations with $M = 256$, at two different monomer densities. The whole box has linear size $L = 50 \sigma$ and periodic boundary conditions while each unit cell of the mesh has linear size $l_s = 10 \sigma$.

III. THEORETICAL CONCEPTS AND OBSERVABLES

In this section we give a brief introduction of the main observables we use throughout the paper. Since we are interested in dynamic and static properties of polymers in solutions we focus our attention to their size and their velocity. The standard measures of these quantities are given by gyration radius $\langle R_g^2 \rangle$ and mean square displacement of the center of mass $\langle \delta \mathbf{r}_{CM}^2 \rangle$, where as usual, $\langle \dots \rangle$ means the average over time and polymers. The gyration radius of a polymer is defined by:

$$R_g^2 = \frac{1}{M} \sum_{i=1}^M [\mathbf{r}_i - \mathbf{r}_{CM}]^2 \quad (7)$$

which simply is the average of the square displacement of each bead from the center of mass \mathbf{r}_{CM} . As already well known from Flory's work on linear polymers[6], we expect that for isolated self-avoiding chains the size scales as:

$$\langle R_g^2 \rangle \sim M^{6/5}. \quad (8)$$

This behaviour is caused by the long-ranged excluded volume interactions, which make the chains behave like self-avoiding random walks (SAW). Since we will focus prevalently on concentrated solutions, where the self-avoiding feature is screened by the presence of other chains, we can simply

get an estimation of the end-to-end distance of the chain by mapping it into a Gaussian chain with bonds equal to the Kuhn length $l_k = 2\xi_p$ [5]:

$$R_e^2 = |\mathbf{r}_M - \mathbf{r}_1|^2 = l_k^2 N_k = l_k \frac{L_c}{l_k} = l_k L_c \quad (9)$$

where $N_k = L_c/l_k$ is the number of Kuhn segments in the chain. Now, using $R_g^2 = R_e^2/6$ we get the Zimm-Stockmayer[18] estimation for an isolated open polymer in solution as

$$R_{g,linear}^2 = \frac{l_k L_c}{6} \quad (10)$$

with an equivalent crude approximation for closed polymers

$$R_{g,rings}^2 = \frac{l_k L_c}{12}. \quad (11)$$

The diffusion of colloids in solution is controlled by the diffusion coefficient D which is related to the temperature T , viscosity η and weight of the colloids M by the Einstein relation:

$$D = \mu(\eta, M) k_B T. \quad (12)$$

In the case of linear polymer in concentrated solution it has been shown[5] that the ‘reptation’ model gives a good description of the system. This model takes inspiration from the snake-like behaviour of the chains in the presence of a fixed network of obstacles. Here, one can imagine tracking only one of the chains, with the rest of the polymers providing constraints on its motion. For very short time-scales (less than the entanglement relaxation time τ_e [5]) the chain does not feel the surrounding obstacles and therefore it freely diffuses until it travels a distance equal to the average distance between the obstacles. For longer time-scales the ‘test’ chain acts like a snake in a background of obstacles, and its motion is constrained to remain in a tube-shaped region (see fig. 4). The diffusion of its center of mass is strongly slowed by the presence of the other chains, and therefore it follows a sub-diffusive, i.e. $t^{1/2}$, dynamics. After the Rouse relaxation time (τ_R), the chain has freed itself from the tube-shaped constraint and the diffusion of the center of mass is again free.

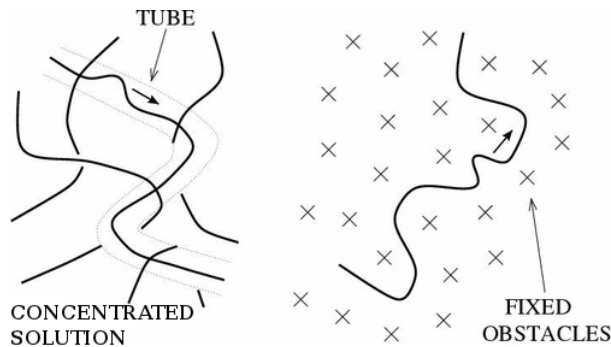


FIG. 4: Cartoon representing the reptation dynamics of an open polymer in concentrated solution.

These three different regimes can be summarised as follows:

$$\langle \delta \mathbf{r}_{CM}^2 \rangle \sim \begin{cases} t & \text{for } t \lesssim \tau_e \\ t^{1/2} & \text{for } \tau_e \lesssim t \lesssim \tau_R \\ t & \text{for } \tau_R \lesssim t \end{cases} \quad (13)$$

where $\langle \delta \mathbf{r}_{CM}^2 \rangle = \langle [\mathbf{r}_{CM}(t) - \mathbf{r}_{CM}(0)]^2 \rangle$. When the dynamics is not constrained one can use the Rouse model for freely diffusive open polymers which gives an expression for the diffusion coefficient of the center of mass D_{CM} [5]:

$$D_{CM}^{Rouse}(M) = \lim_{t \rightarrow \infty} \frac{\langle \delta \mathbf{r}_{CM}^2 \rangle}{6t} = \frac{k_B T}{M\gamma} \quad (14)$$

which, under the conventions fixed above, i.e. $k_B T = \gamma = 1$, it reduces simply to $D_{CM}^{Rouse} = M^{-1}$. In fig. 5 we show the scaling behaviour of the size of isolated rings in solution with M beads and their mean square displacement for the cases $M = 600$ and $M = 200$, together with their expected Rouse behaviour.

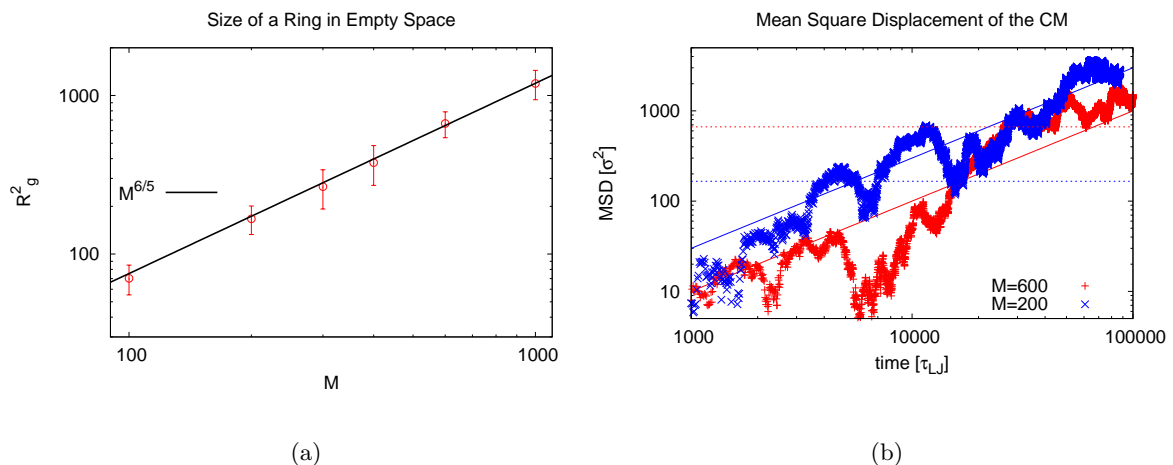


FIG. 5: (a) Data points represent the mean square gyration radius $\langle R_g^2 \rangle$ as a function of the molecular mass M for isolated ring polymers in empty space. The error bars are calculated as $\langle \delta R_g^2 \rangle = (\langle R_g^4 \rangle - \langle R_g^2 \rangle^2)^{1/2}$. The scaling behaviour for self-avoiding random walk $R_g^2 \sim M^{6/5}$ is represented by the black line. (b) Mean square displacement of the center of mass as a function of the time τ_{LJ} . The solid lines have slope $\langle \delta \mathbf{r}_{CM}^2 \rangle / t = 6/M$ while the dotted lines represent the average value of the radius of gyration (blue for $M=200$, red for $M=600$).

IV. DILUTE SOLUTIONS OF RINGS IN A MESH

A. Isolated Polymers

In this section we consider properties of ring polymers in presence of the gel. As we have already mentioned, embedding a polymer solution in a network of fixed obstacles is interesting because it can give useful insight on the behaviour of concentrated solutions immersed in, for instance, agarose, which is a gel widely used to perform DNA electrophoresis. As far as we know, simulations in these conditions have not yet been performed, despite their simplicity. In addition to this, such systems mimic polymer solutions in which two types of polymers are present, one much longer and heavier (i.e. background of obstacles) than the other (i.e. rings).

We first want to study the static properties of closed and open isolated polymers in the presence of the gel. For a linear polymer it has been shown[2] that its size would scale as if it was in empty

space, i.e. $R_g \sim M^{3/5}$. For a ring polymer instead, we can use a fundamental result of Parisi and Sourlas [14]. These authors have showed that a long closed polymer in a network of fixed obstacles belongs to the same universality class as a branched polymer. Moreover, it has been shown that the exponent of large branched diluted polymers in D dimensions are related to the exponents of the Lee-Yang singularity of the Ising model in $D-2$ dimensions. From the exact solutions of the Ising model in one dimension one can get the critical exponent for the size of ring polymers in three dimensions, which scales as $R_g \sim M^{1/2}$. As far as we know, this fundamental result has not yet been reproduced computationally, despite it being one of the few exact values known for critical exponents in three dimensions. In fig. 6 we show R_g^2 as a function of M for both ring and linear polymers in dilute conditions, where the chains are essentially isolated. In fig. 7 we show different configurations adopted by ring polymers in the presence or absence of the gel.

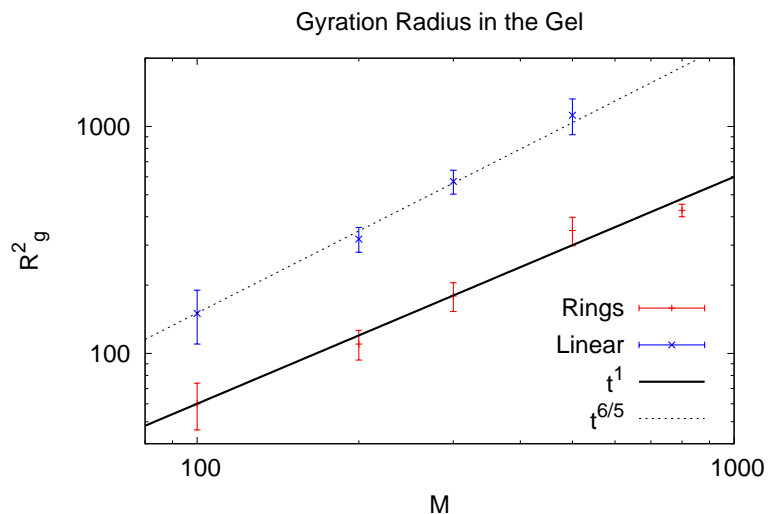


FIG. 6: Data points represent the mean square gyration radius $\langle R_g^2 \rangle$ as a function of the polymer weight M for isolated polymers in presence of the mesh. The persistence length of the chains was kept at $\xi_p = 5\sigma$ and the linear size of the box at $L = 100\sigma$. Error bars are given by $\langle \delta R_g^2 \rangle = \sqrt{\langle R_g^4 \rangle - \langle R_g^2 \rangle^2}$. Dotted line represents self-avoiding random walk behaviour, while solid line represents the critical exponent predicted in [14].

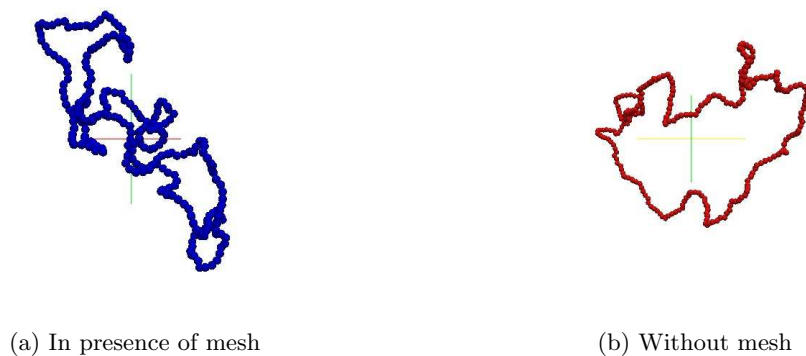


FIG. 7: Two different chain configuration in presence (a) and in absence (b) of the mesh. One can already see that in dilute conditions the configuration of the ring embedded in the mesh is more snake-like than the one in an empty space. This is because each lattice volume must contain both an outgoing and returning portions of the ring contour, while there is no such constraint in the absence of the gel.

B. Low Concentration Solutions

In this section we study three systems with same monomer density $\rho = 0.02\sigma^{-3}$ but different packing fractions, defined by $\phi = 4\pi N\langle R_g^2 \rangle^{3/2}/3V$, where V is the volume of the box, which has linear size $L = 50\sigma$ and periodic boundary conditions. Below we report the observed values of the gyration radius and the consequent packing fraction ϕ .

	No Gel			Gel		
	N=10, M=256	N=20, M=128	N=40, M=64	N=10, M=256	N=20, M=128	N=40, M=64
R_g^2	188.2	88	38.8	133.5	69.9	33.5
ϕ	0.836	0.54	0.29	0.5	0.37	0.25

The presence of the gel decreases the size of the rings at this monomer density. For higher monomer densities it has been shown that the size of large rings behaves like that of crumpled globules[8, 17]. Notice that in this case, the presence of the gel with lattice constant $l_s < L_c$ together with the polymer stiffness forbids the rings to segregate and behave like collapsed globules. The packing fraction ϕ gives a measure of the degree of coil overlap. For $\phi \ll 1$, we can comfortably fit N balls with radius R_g into the box, otherwise, for $\phi \gg 1$ the balls would overlap. Here this would mean that the rings would have a greater probability of inter-penetration.

Dynamics

In this section we show how the presence of the gel affects the motion of the molecules in the solution. We find that the presence of gel makes the diffusion slower. We can incorporate this effect into the expression for the diffusion coefficient D_{CM}^{Rouse} simply by substituting the friction γ with an effective friction γ_0 , to be calculated from the simulations. Obviously, γ_0 would depend on the size of the polymers, since the slowing of the motion is due to topological interaction between chains and gel. In fig. 8, 9 and 10 we compare the behaviour of the mean square displacement of the center of mass (MSD) $\langle \delta r_{CM}^2 \rangle$ in the presence and in absence of the gel. From these plots one can notice that γ and γ_0 get closer as we consider shorter chains. In other words, the diffusion coefficient for long time-scales is dependent on the fact that a mesh is present, and this effect is less important for shorter chains. This is due to the fact that shorter chains tend to interact less with both, other rings and the background mesh.

Figures 8, 9 and 10 can be well explained in terms of reptation dynamics[5]. In fact, when the lattice of obstacles is absent, the mean squared displacement of the rings diffusing in the box is linear throughout the time window. Since the solution is dilute, we expect that entanglement effects are not important in the system. Therefore, we expect that the rings undertake free diffusion even at short time scales. On the contrary, the presence of the mesh provides a sort of natural tube, in which the rings are forced to reptate. As a consequence, we get the three regimes (as in eq. 13) which we show in fig. 11, as predicted by the reptation model. In the same figure we also highlight the crossover from t^1 to $t^{1/2}$ resulting in an intermediate scaling of $t^{0.75}$ as already observed in [9], and better shown in fig. 12 where we plot $M\langle \delta r_{CM}^2 \rangle$ resulting in a collapse of the curves.

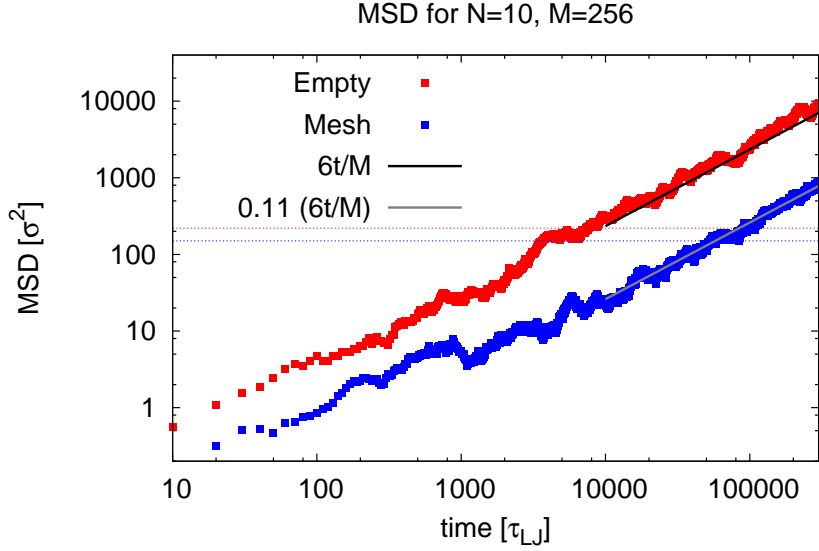


FIG. 8: Filled squares: Mean square displacement of the center of mass for $N = 10$ and $M = 256$ in presence (blue) and absence (red) of the gel. Blue and red dotted lines represent correspondent values of $\langle R_g^2(M) \rangle$. Solid black line: Rouse behaviour for $\langle \delta r_{CM}^2 \rangle$. Solid grey line: In presence of the mesh $\gamma_0(M = 256) \sim 9 \gamma$, which makes $D_{CM}^{Mesh} = 0.11 D_{CM}^{Rouse}$.

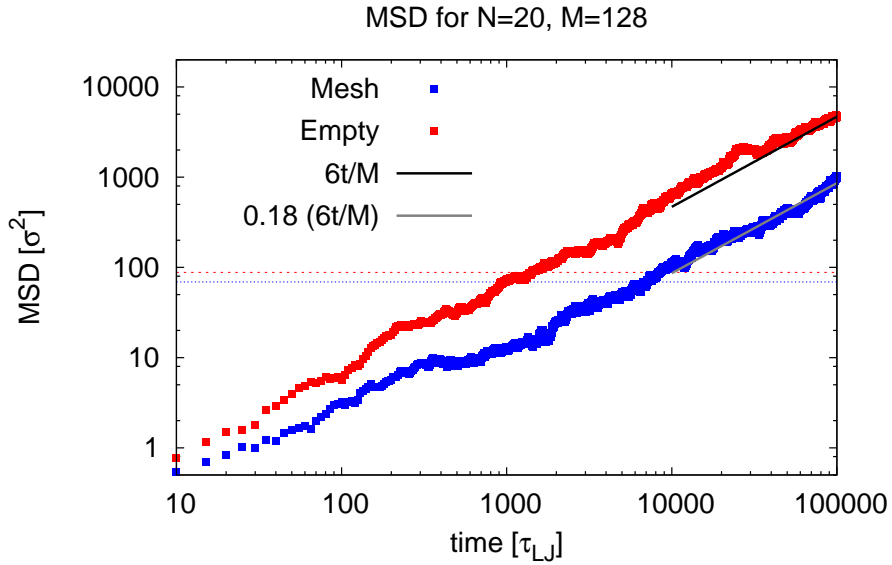


FIG. 9: Filled squares: Mean square displacement of the center of mass for $N = 20$ and $M = 128$ in presence (blue) and absence (red) of the gel. Blue and red dotted lines represent correspondent values of $\langle R_g^2(M) \rangle$. Solid black line: Rouse behaviour for $\langle \delta r_{CM}^2 \rangle$. Solid grey line: In presence of the mesh $\gamma_0(M = 128) \sim 5.5 \gamma$, which makes $D_{CM}^{Mesh} = 0.18 D_{CM}^{Rouse}$.

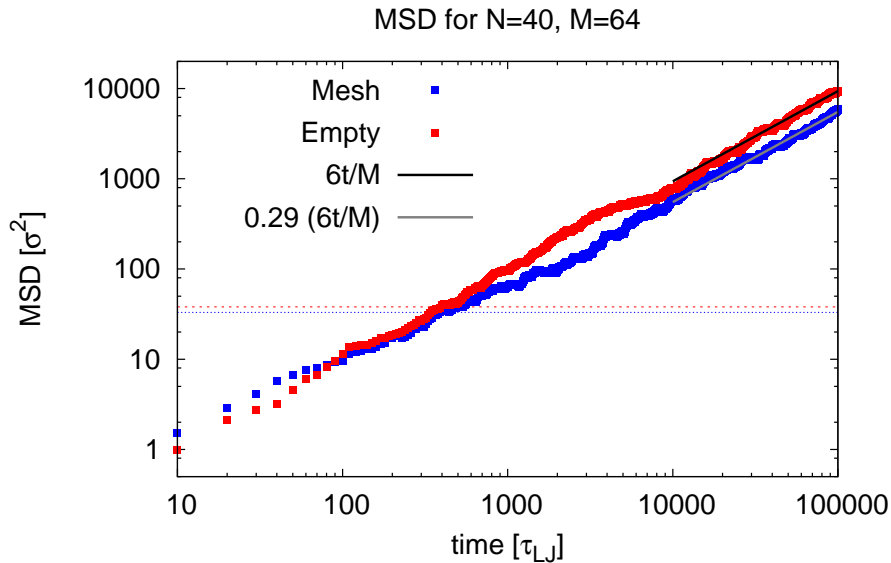


FIG. 10: Filled squares: Mean square displacement of the center of mass for $N = 40$ and $M = 64$ in presence (blue) and absence (red) of the gel. Blue and red dotted lines represent correspondent values of $\langle R_g^2(M) \rangle$. Solid black line: Rouse behaviour for $\langle \delta r_{CM}^2 \rangle$. Solid grey line: In presence of the mesh $\gamma_0(M = 64) \sim 3.4\gamma$, which makes $D_{CM}^{Mesh} = 0.29 D_{CM}^{Rouse}$

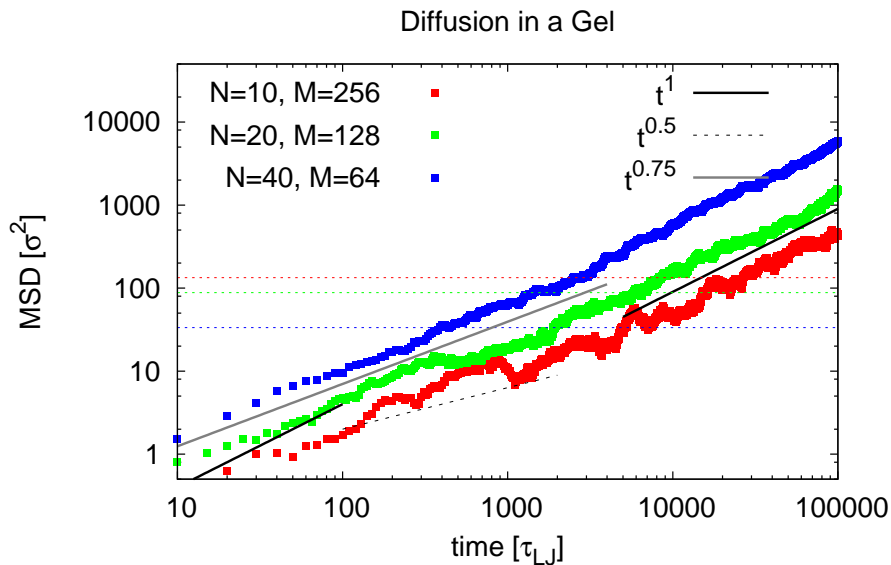


FIG. 11: Filled Squares: Mean square displacement of the center of mass for the three different samples. Dotted coloured line: $\langle R_g^2(M) \rangle$. Solid black line: free diffusive behaviour. Dotted black line: Sub-diffusive behaviour for short time-scales. Solid grey line: Intermediate behaviour $t^{0.75}$ evident for shorter chains.

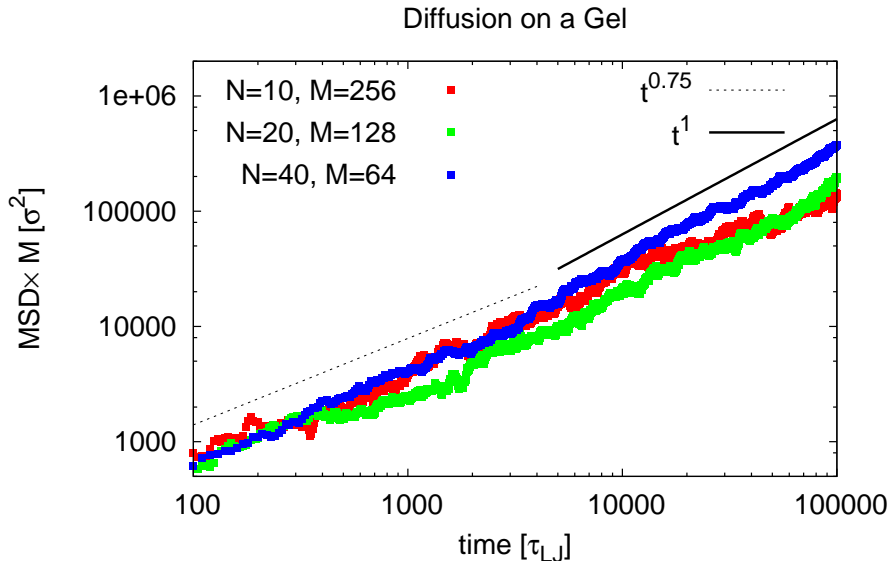


FIG. 12: Filled Squares: Mean square displacement of the center of mass multiplied by the size of the chains M for the three different samples. Solid black line: free diffusive behaviour. Dotted black line: Intermediate behaviour $t^{0.75}$.

V. SEMI-DILUTE SOLUTIONS IN OVERLAPPING REGIME

In this section we aim to increase the packing fraction $\phi = 4\pi N \langle R_g^2 \rangle^{3/2} / 3V$ keeping the monomer concentration $\rho = MN/V$ small. We choose to work with the three following system parameters: (1) $L = 50\sigma, N = 50, M = 256$, (2) $L = 60\sigma, N = 30, M = 512$, (3) $L = 100\sigma, N = 50, M = 1024$. The expected value for ϕ is the same in all the three cases and greater than one: $4\pi(L_c l_k / 12)^{3/2} N / 3V \sim 5$, nevertheless $\rho \lesssim 0.1$. The fact that the monomer density is small has a couple of important advantages. First, previous works on ring polymer have always been conducted at high monomer density which can be the cause of the high degree of ring segregation observed for instance in [8] and [17]. Since we want the rings to interact between each other, we keep the monomer density low to avoid such phenomenon. Secondly, despite the fact that the solution is highly packed, the simulation time is relatively small, compared to that required for higher ρ .

Below, we report the measured values of the gyration radius and the packing fraction. In fig. 13 we show the behaviour of the mean square displacement of the center of mass for two cases. In this plot one can notice that ratio D_{CM} / D_{CM}^{Rouse} for the case $N = 50$ and $M = 256$ is smaller than the one found in the previous section for $N = 10$ and $M = 256$. This suggests that increasing the packing fraction ϕ makes the polymers interact more, as one would expect. In fig. 14 we show how the ratio D_{CM} / D_{CM}^{Rouse} depends on the packing fraction ϕ . In order to justify the monotonic decreasing of the diffusion coefficient as a function of ϕ one can think about the cartoon (see fig. 1) we sketched at the beginning of the paper. As the coils get more packed and the chains longer, the probability of inter-ring entanglement/penetration increases, causing an important slowing of the motion. In the next section we will present a method to unambiguously identify the type of topological constraints affecting the rings and to relate it with the slowing of the motion.

	L=50 σ , N=50, M=256	L=60 σ , N=30, M=512	L=100 σ , N=50, M=1024
R_g^2	109	450	1200
ϕ	1.9	5.4	9.1

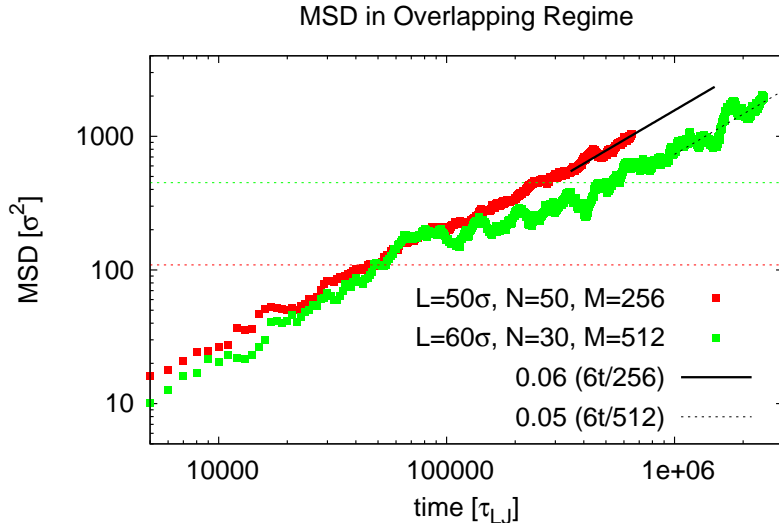


FIG. 13: Mean square displacement for two of the systems in overlapping regime. Solid line: Linear regression for $N = 50$, $M = 256$ which gives $D_{CM}/D_{CM}^{Rouse}(M = 256) = 0.06$. Dotted line: Linear regression for the system $N = 30$, $M = 512$ which gives $D_{CM}/D_{CM}^{Rouse}(M = 512) = 0.05$.

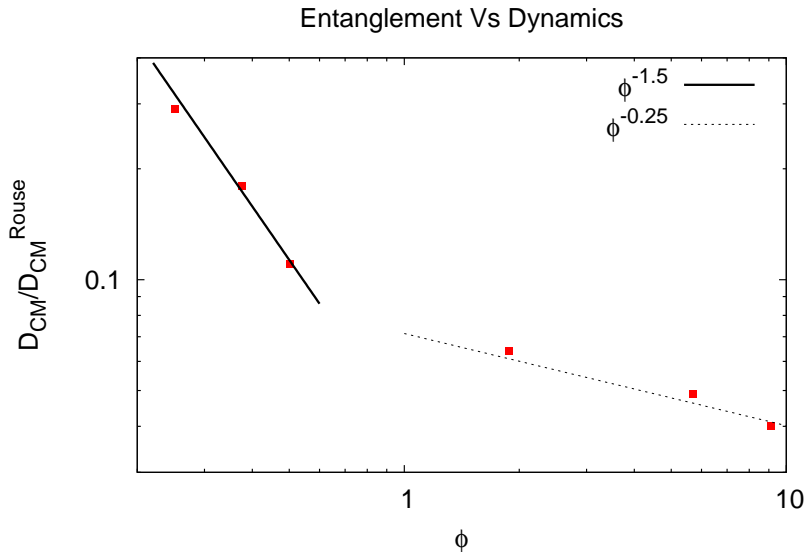


FIG. 14: Ratio D_{CM}/D_{CM}^{Rouse} as a function of ϕ . Notice the sudden change on the behaviour of D_{CM}/D_{CM}^{Rouse} as soon as the value $\phi_c = 1$ at which the chains start to overlap, is crossed.

VI. TOPOLOGICAL INTERACTIONS: LINKING AND THREADING NUMBERS

In this section we want to exploit the presence of the gel to measure the topological constraints involving threading between different ring polymers. This effect, in which rings penetrate through each-other has long been debated, and it is not still clear whether it has a major role in slowing the

dynamics of pure ring solutions (while a similar effect has already been observed in mixed solutions of rings and linear polymers [3]). If observed, it would cause a much longer relaxation time, due to the fact that rings would have to unthread themselves before being able to reptate along the tube. Having in mind that we want to relate the dynamics of the rings to their entanglements and/or penetrations, we here suggest two strategies to measure the existence of such constraints. The first strategy has already been used in [12] and [13] and does not strictly require that the solution is made of ring polymers or the presence of the gel. The second strategy is a slight modification of the first that exploits the fact that we are dealing with ring polymers embedded in a background gel.

A. Linking Number

The first strategy we implement is as follows:

- We consider a unit box, i.e. a box defined by the lattice gel, and identify the strands passing through it, as belonging to the same ring or different rings. Every strand has an entry point \mathbf{r}_{in} and an exit point \mathbf{r}_{out} ;
- We choose a direction along which we are going to close the strand to form a new ring based on the following prescription: if \mathbf{r}_{in} and \mathbf{r}_{out} lay on the same face, or opposite faces with normal \hat{n} , we arbitrarily choose one of the two directions perpendicular to \hat{n} . We then assign an orientation ± 1 depending on the position of the center of mass of the strand. If the strand mainly lays on the bottom (top) half of the unit box in direction \hat{m} we'd choose a final direction $-\hat{m}$ ($+\hat{m}$) (where $\hat{m} \perp \hat{n}$). If they lay on adjacent faces with normals \hat{m} , \hat{k} , we arbitrarily choose one between \hat{m} and \hat{k} and again we assign the orientation based on the position of the strand center of mass along the chosen direction;
- Once that the direction is chosen (say \hat{m}), we join the ends \mathbf{r}_{in} and \mathbf{r}_{out} following a path outside the unit box; in particular, we add a distance equal to one mesh lattice size l_s to both \mathbf{r}_{in} and \mathbf{r}_{out} along \hat{m} and we then join the points $\mathbf{r}_{in} + l_s\hat{m}$ and $\mathbf{r}_{out} + l_s\hat{m}$ following the shortest path between them.

Examples of the procedure for one strand and for all of them are shown in fig. 15 and 16.

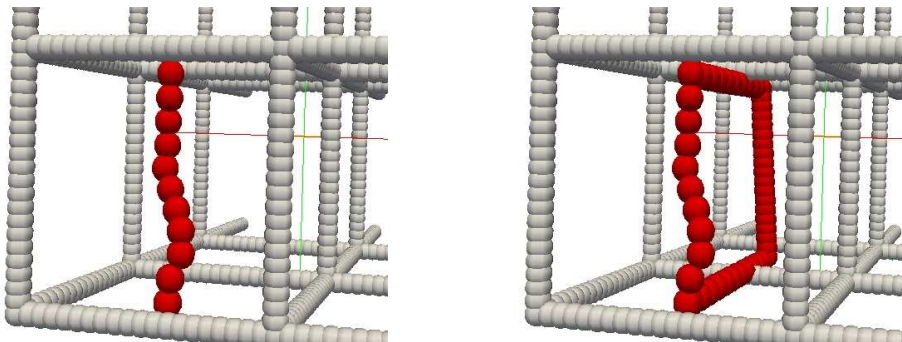


FIG. 15: Joining the ends of a strand following the procedure described above.

It is worth noticing that it does not matter if we cross the edges of the mesh when we join the strands, because once that the new set of rings has been created inside a mesh volume (made upon the closed strands), we discard the mesh and simply compute the linking number (Lk) between each

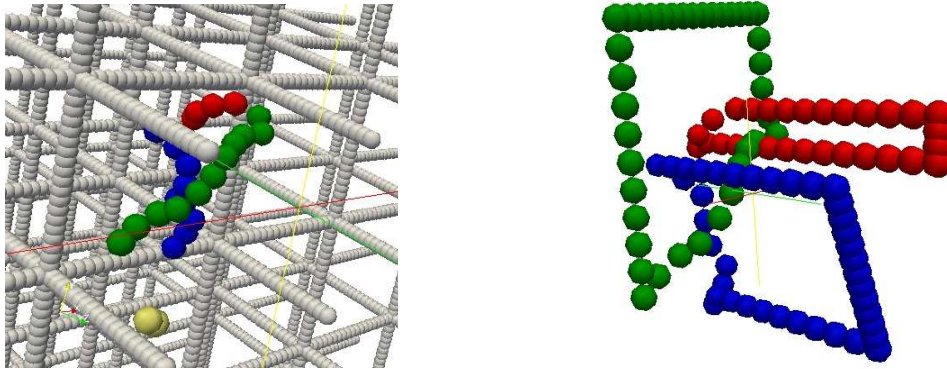


FIG. 16: Joining the ends of the strands in a unit box following the procedure explained above results in a new set of rings which can be linked or unlinked. The sum of the linking number between each pair gives a measure of the degree of entanglement.

pair of new rings (for instance in fig. 16 we would get $Lk = 2$, since the blue and red rings are linked with the green one). In this way, we can give a simple, but arbitrary, measure of the entanglements felt locally by the chains. This procedure does not distinguish the intra-chain entanglements from the inter-chain entanglements, nor between entanglement and penetration. Above we stressed the fact that this measure is arbitrary, since one has to follow a procedure to choose a closing direction which is not unique nor justifiable physically. Nevertheless, we will show later that changing the choice of the direction will have, on average, similar results.

B. Threading Number

The following strategy for measuring inter-ring penetration exploits the existence of a background of fixed obstacles arranged in an ordered fashion. This constrains the rings to assume only certain configurations. In particular, as one can see in fig. 17, in order to conserve the topological state and remain unlinked from the structure of the gel, the rings must not cross the edges of the mesh. As a consequence, for each unit box visited by a polymer there must be, at least, a pair of entry points and a pair of exit points. In addition to that, each pair must lay on the same face.

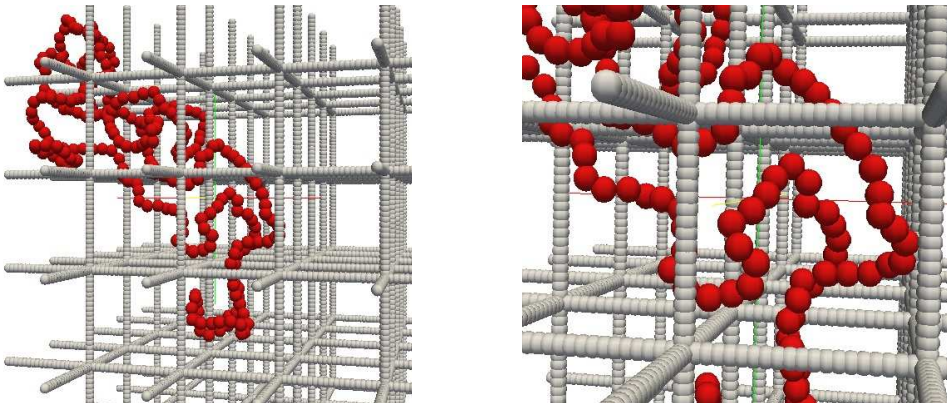


FIG. 17: Example of the configuration of a ring in a background mesh. The ring configuration is reminiscent of the shape of a snake moving through obstacles. Notice that due to the topological constraints there always are a pair of strands passing through the faces of the unit boxes.

We can take advantage of this limitation on the possible configurations in order to suggest the following strategy to compute, unambiguously, the threading number Th between a pair of chains,

which takes value 1 if two chains are penetrating through each other, 0 if they are not.

- We consider the strands visiting a unit box (defined by the lattice space l_s) with entry points $\mathbf{r}_{in,1}^i, \mathbf{r}_{in,2}^i$ and exit points $\mathbf{r}_{out,1}^i$ and $\mathbf{r}_{out,2}^i$, where i runs over the number of different rings (not strands!) passing through the box.
- If a chain has got excursions outside the box, they define a new pair of points $\mathbf{r}_{e,1}^i, \mathbf{r}_{e,2}^i$. Since the sum of entry, exit and excursion points must be even, we can join the point $\mathbf{r}_{j,1}^i$ with the point $\mathbf{r}_{j,2}^i$ following the shortest path, and where j runs over the kind of points (in, out, e).
- Once the points have been joined, a new ring i' is created, which is made by the strands of i belonging to the unit box plus the segments joining the end points.
- Once a new ring i' has been created, we consider the strands s which do not belong to the ring i and close them very far away from the box by adding a large number of beads along the direction defined by the last couple of beads belonging to the unit cell and joining the far ends following the shortest path. In this way we generated new closed loops s' .
- If a ring threads the ring i , then there must be a couple of strands passing inside the new ring i' . Therefore, we compute the linking number between i' and the set of s' and divide by 2. If $Th = \sum_{s'} Lk(i', s')/2$ is 1, then it is evident that a ring is threading i' and therefore i as well.
- We repeat the same strategy for each ring visiting each unit box and sum all the Th .

In fig. 18 we show an example of the application of this method. In this case the blue ring penetrates the red one. After we apply the procedure described above, we obtain a new red/orange ring made by the original (red) segments plus the orange ones connecting the end points. The blue strands are closed far away from the unit box with the light blue beads.

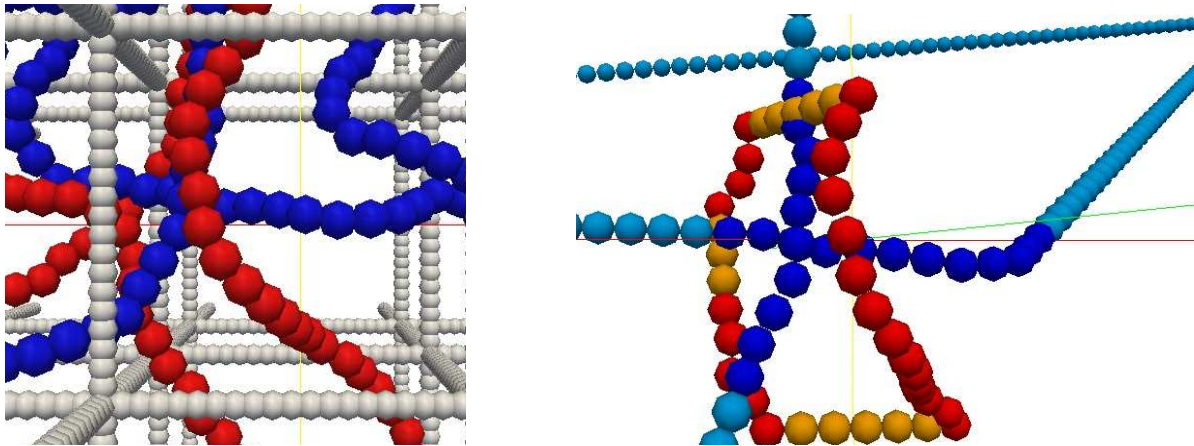


FIG. 18: Example of the method described above, where red strands are joined to form a red/orange ring and blue strands are closed at infinity to form blue/cyan loops. The value of $Th = \sum_{blue/cyan} Lk(red/orange, blue/cyan)/2$ is equal to 1.

The procedure described above does not require any arbitrary choice, on the other hand, it is not flawless. Sometimes the threading can occur across two unit boxes, and in that case our procedure would give an anomalous result, i.e. it would give a non integer value for Th . If that happens,

we do not include it as a penetration as we seek only unambiguous examples of the existence of such threading. Moreover, we also check that the new rings i' are not linked between each other. If that is not the case, we discard the value for Th obtained in that unit box, due to ambiguous configurations of the chains.

C. Results

The results of these two methods applied on a number of systems is shown in table I. We report the values of the time average value of the linking number in the whole box divided by the number of chains in the system. We also report the value of Lk obtained considering a different choice of the closing direction \hat{m} (in brackets below). The time average of the threading number is also reported. The last column in table I indicates the time average of the number of different chains visiting a unit box.

N	M	L	ξ_p	$\langle R_g^2 \rangle$	ϕ	$\langle Lk \rangle / N$	$\langle Th \rangle$	$\langle \text{Rings} \rangle / ub$
40	64	50	5	33	0.25	0.35(0.32)	1.6	1.2
20	128	50	5	70	0.37	0.9(0.9)	1.3	0.97
10	256	50	5	133	0.5	1.9(1.9)	0.9	0.97
50	256	50	5	109	1.8	5.3(5.9)	32	4.6
30	512	60	5	450	5.4	10.5(9.5)	20	2.6
50	1024	100	5	1200	9.1	22.0(21.3)	41.5	1.75

TABLE I: Values of linking number and threading number calculated as described in above together with packing fraction and average number of different chains per unit box for the system parameters here considered.

One can notice that the calculation of the linking number $\langle Lk \rangle$ following the procedure described above with two different choices of the direction \hat{m} along which we close the strands gives very similar results. This implies that, on average, the choice does not affect the outcomes. In addition to that, it is clear that the value of $\langle Lk \rangle / N$ is monotonically increasing with the packing fraction ϕ (see fig. 19a) and the rings length M (see fig. 19b), as we expected. These plots strongly suggest that the number of entanglements experienced by each ring scales with the length of the ring. While it is not clear what is the functional form $Lk(\phi)$. Nevertheless, it is evident that a transition occurs when the overlapping value $\phi_c = 1$ is crossed.

One can also see that for the first set of parameters, the threading number $\langle Th \rangle$ is very small. This is because these systems have packing fraction below $\phi_c = 1$, and therefore the rings can occupy a non-overlapping space in the volume V . Moreover, since $\langle Th \rangle$ measures the threading only between different rings, by reducing the number of rings in solution we expect a decreasing of the probability of inter-ring penetration. The same effect can be observed in the second set of parameters, where the system with $N = 30$ and $M = 512$ has a smaller $\langle Th \rangle$ with respect to the other two systems which have a larger N . A part from the case with parameters $L = 100\sigma$, $N = 50$ and $M = 1024$ we also observe that the average number of different chains visiting a unit box is closely related to $\langle Th \rangle$. Again, this is due to fact that Th measures only inter-ring penetrations. The last case represents an exception to a very evident behaviour. This strongly suggests that in this case, the inter-ring penetrations is very close to be percolating through the entire system, since $\langle Th \rangle / N \sim 1$. In other words, in this case one can think to have very long rings spanning many unit boxes and threading, on average, through at least one other ring, creating an extended grid made of penetrating rings.

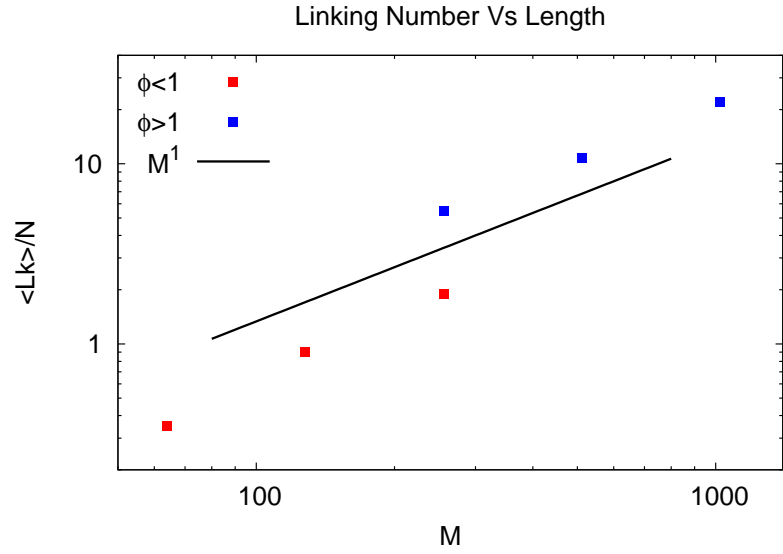
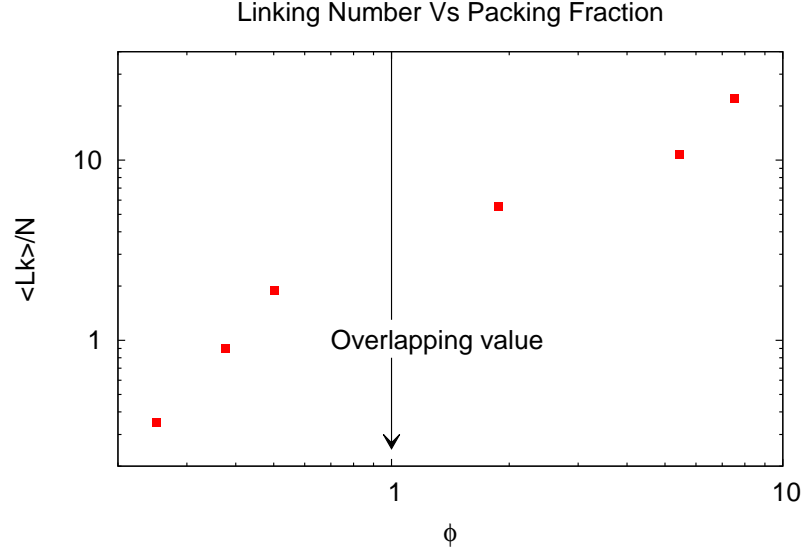


FIG. 19: Linking number $\langle Lk \rangle$ as a function of the packing fraction ϕ (a) and length of the rings M (b). It is worth noticing that $\langle Lk \rangle$ increases linearly with M for both sets of systems, below (red) and above (blue) overlapping. From (a) one can see a discontinuous behaviour as we cross ϕ .

In order to relate the slowing of the dynamics with the topological entanglements between rings we plot in fig. 20 the ratio D_{CM}/D_{CM}^{Rouse} as a function of the linking number $\langle Lk \rangle/N$. As one can see, diffusion coefficient D_{CM} decreases monotonically with the number of entanglements per

chain. In particular we obtain that the ratio D_{CM}/D_{CM}^{Rouse} scales as $(\langle Lk \rangle/N)^{-1/2}$. Since the threading number varies with the number of chains in the system, we do not obtain a similar relationship between D_{CM}/D_{CM}^{Rouse} and $\langle Th \rangle$, despite the fact that we have showed the existence of such phenomenon. As future work, we might want to focus on studying systems with fixed number of chains and check whether the threading number has similar effects on the dynamics and whether this increases with the length of the rings.

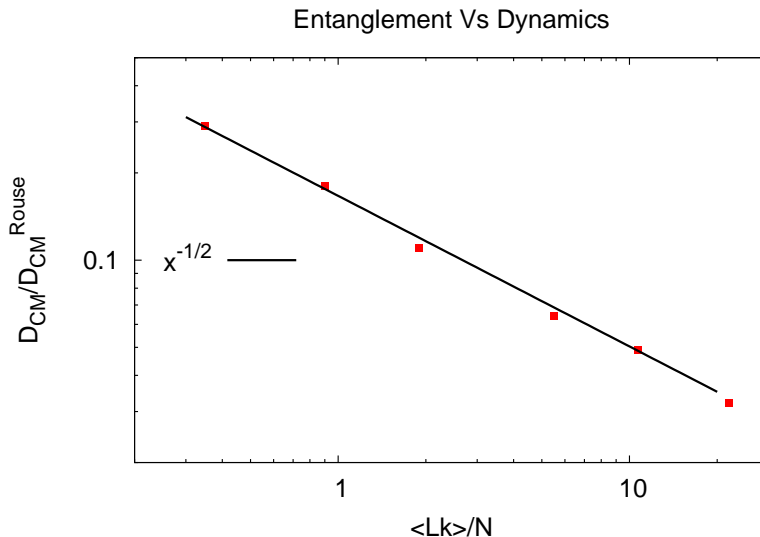


FIG. 20: Ratio D_{CM}/D_{CM}^{Rouse} as a function of the linking number $\langle Lk \rangle$ for the system parameters in table I.

VII. CONCLUSIONS

In this work we reported the results obtained from molecular dynamic simulations carried out with solutions of polymer rings in a background mesh. We used a bead-spring model to simulate semi-flexible unknotted and unlinked rings in solution at fixed volume and temperature. In sec. IV we have computationally observed that the size of isolated rings in a background of fixed obstacles (mesh) scales as $M^{1/2}$ according with the exponent predicted by Parisi and Sourlas in [14]. While isolated linear polymers behave as they were in empty space, i.e. as self-avoiding random walkers. In sec. IV and V we then observed the behaviour of the mean square displacement of the center of mass of the polymers. In agreement with Doi and Edwards' reptation model[5], $\langle \delta r_{CM}^2 \rangle$ shows three different regimes. We also computed the effective diffusion coefficient D_{CM} for long time scales and compared it with the diffusion coefficient D_{CM}^{Rouse} predicted using the Rouse model for freely diffusive linear polymers. In sec. VI we then formulated a strategy to measure the topological entanglements between the polymers and proposed a new observable Th able to identify uniquely inter-chain penetrations. These observables have been related to the system properties, as polymer length and packing fraction. As we expected, there is a linear relationship between entanglement and length of the rings (see fig. 19b). A similar result was expected for the threading Th , nevertheless we did not obtain a clear functional form $Th(M)$ due to the fact that

we changed the number N of rings in the system. As we explained above, this observable captures only penetrations between different rings, and therefore by changing N we biased the outcome. Future work will comprehend the study of a system with $L = 70\sigma$, $N = 50$, $M = 512$ such that $\phi > 1$ and Th can be compared with that obtained for the other systems with same $N = 50$. These observables have also been related to the dynamics of the rings, using the ratio D_{CM}/D_{CM}^{Rouse} , which gives a measure of the slowing of the dynamics of the rings in solution at long time scales. As we expected, the entanglement degree is closely related to the slowing of the dynamics, since the rings can never be completely disentangled from the other rings in solution. As a future work we might want to obtain a similar functional form for the threading number. More precisely, instead of observing the long time scale dynamics, we expect that the threading mechanism increases dramatically the Rouse relaxation time τ_R , since the rings must unravel themselves before to reptate.

The results presented here offer some insights on the challenging problem of relating dynamics and topological properties of rings in solution. As far as we know, the computation of the observables described in sec. VI has never been carried out on three dimensional molecular dynamics simulations. In addition to this, the results obtained suggest that a percolating threading spanning the whole system might occur for very long polymers in overlapping regime with low monomer density ρ , as in the system with $L = 100\sigma$, $N = 50$ and $M = 1024$. Thanks to the strategy we proposed to compute Th we would be able to identify whether such mechanism is responsible for the occurring of a new state of matter such as a topological glass.

In summary, here we have suggested a new method to study rings in a gel. As far as we know we also have developed an original strategy to unambiguously quantify penetrations that exploits the geometry of the mesh. This method can give a better understanding of a long debated problem as the relationship between topological constraints and dynamics in polymer rings in solution. We have also showed that penetrations do actually occur between rings, even if we here employed only modest simulation parameters. As we have already mentioned, our findings are strongly suggestive of the emergence of a topological glass for long enough rings above overlap concentration, the observation of which would have an important impact on formulating new theories for ring polymers.

-
- [1] BROWN, S., AND SZAMEL, G. Structure and dynamics of ring polymers. *The Journal of Chemical Physics* 108, 12 (1998), 4705.
 - [2] CATES, M., AND DEUTSCH, J. Conjectures on the statistics of ring polymers. *Journal de physique* 47 (1986), 2121–2128.
 - [3] CHAPMAN, C., AND SHANBHAG, S. Complex effects of molecular topology on diffusion in entangled biopolymer blends. *Soft Matter* 8, 35 (2012), 9177.
 - [4] CREMER, T., AND CREMER, C. Chromosome territories, nuclear architecture and gene regulation in mammalian cells. *Nature reviews. Genetics* 2, 4 (Apr. 2001), 292–301.
 - [5] DOI, M., AND EDWARDS, S. *The theory of polymer dynamics*. 1988.
 - [6] FLORY, P. *Principles of polymer chemistry*. 1953.
 - [7] GENNES, P. D. *Scaling concepts in polymer physics*. 1979.
 - [8] HALVERSON, J. D., LEE, W. B., GREY, G. S., GROSBERG, A. Y., AND KREMER, K. Molecular dynamics simulation study of nonconcatenated ring polymers in a melt. I. Statics. *The Journal of chemical physics* 134, 20 (May 2011), 204904.
 - [9] HALVERSON, J. D., LEE, W. B., GREY, G. S., GROSBERG, A. Y., AND KREMER, K. Molecular dynamics simulation study of nonconcatenated ring polymers in a melt. II. Dynamics. *The Journal of*

- chemical physics* 134, 20 (May 2011), 204905.
- [10] KREMER, K., AND GRETT, G. S. Dynamics of entangled linear polymer melts: A molecular-dynamics simulation. *The Journal of Chemical Physics* 92, 8 (1990), 5057.
 - [11] LEE, H. C., LEE, H., LEE, W., CHANG, T., AND ROOVERS, J. Fractionation of Cyclic Polystyrene from Linear Precursor by HPLC at the Chromatographic Critical Condition. *Macromolecules* 33, 22 (Oct. 2000), 8119–8121.
 - [12] ORLANDINI, E. Polymer entanglement in melts. *Journal of Physics A: ...* 181 (2000).
 - [13] ORLANDINI, E., AND WHITTINGTON, S. G. Entangled polymers in condensed phases. *The Journal of chemical physics* 121, 23 (Dec. 2004), 12094–9.
 - [14] PARISI, G., AND SOURLAS, N. Critical behavior of branched polymers and the Lee-Yang edge singularity. *Physical Review Letters*, 14 (1981), 871–874.
 - [15] ROSA, A., ORLANDINI, E., AND TUBIANA, L. Structure and dynamics of ring polymers: entanglement effects because of solution density and ring topology. *Macromolecules* (2011), 8668–8680.
 - [16] RUBINSTEIN, M., AND COLBY, H. R. *Polymer Physics*. Oxford University Press.
 - [17] VETTOREL, T., GROSBERG, A. Y., AND KREMER, K. Statistics of polymer rings in the melt: a numerical simulation study. *Physical biology* 6, 2 (Jan. 2009), 025013.
 - [18] ZIMM, B. H., AND STOCKMAYER, W. H. The Dimensions of Chain Molecules Containing Branches and Rings. *The Journal of Chemical Physics* 17, 12 (1949), 1301.